

CountZES: Counting via Zero-Shot Exemplar Selection

Muhammad Ibraheem Siddiqui Muhammad Haris Khan
Mohamed Bin Zayed University of Artificial Intelligence
{muhammad.siddiqui, muhammad.haris}@mbzuai.ac.ae

Abstract

Object counting in complex scenes remains challenging, particularly in the zero-shot setting, where the goal is to count instances of unseen categories specified only by a class name. Existing zero-shot object counting (ZOC) methods that infer exemplars from text either rely on open-vocabulary detectors, which often yield multi-instance candidates, or on random patch sampling, which fails to accurately delineate object instances. To address this, we propose CountZES, a training-free framework for object counting via zero-shot exemplar selection. CountZES progressively discovers diverse exemplars through three synergistic stages: Detection-Anchored Exemplar (DAE), Density-Guided Exemplar (DGE), and Feature-Consensus Exemplar (FCE). DAE refines open-vocabulary detections to isolate precise single-instance exemplars. DGE introduces a density-driven, self-supervised paradigm to identify statistically consistent and semantically compact exemplars, while FCE reinforces visual coherence through feature-space clustering. Together, these stages yield a diverse, complementary exemplar set that balances textual grounding, count consistency, and feature representativeness. Experiments on diverse datasets demonstrate CountZES superior performance among ZOC methods while generalizing effectively across natural, aerial and medical domains. Code is available at [GitHub](#).

1. Introduction

Object counting plays a vital role in a wide range of applications, including crowd and traffic analysis [15], agriculture [5], and biomedical microscopy [34]. Traditional counting approaches are typically *class-specific*, tailored for predefined categories such as crowds [2], vehicles [18], or cells [35]. However, these methods require retraining whenever a new class is introduced, limiting their scalability. To overcome this, *class-agnostic counting* has emerged, aiming to generalize to unseen categories [10, 12, 38]. Existing class-agnostic methods can be categorized into three paradigms: *few-shot object counting* (FSOC), *reference-*

Performance across Natural, Aerial and Medical Domains

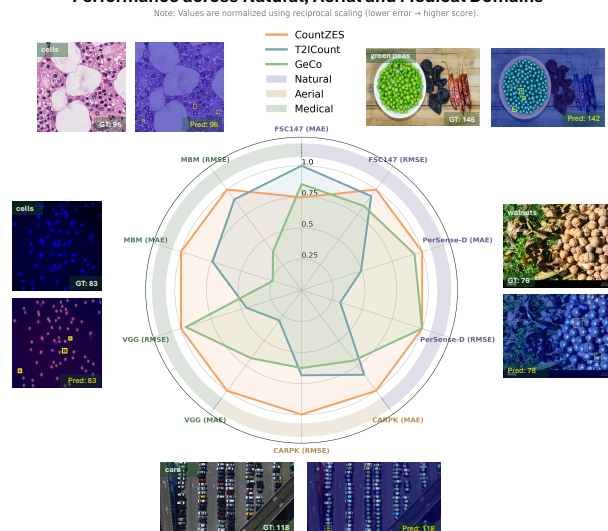


Figure 1. Zero-shot object counting comparison of our CountZES against recently proposed T2ICount [28] and GeCo [26] across diverse benchmarks spanning natural, aerial, and medical domains.

less counting (RLC), and *zero-shot object counting* (ZOC).

FSOC methods rely on a small set of annotated exemplars provided at inference [7, 24, 38], which limits scalability [39, 40]. In contrast, RLC estimates counts directly from global visual cues [4, 8, 20, 30], but lacks semantic awareness and tends to focus on visually dominant patterns [37, 41]. To address these issues, ZOC has emerged as a promising direction [13, 14, 37, 41], enabling the counting of arbitrary unseen categories from text prompts alone.

Current ZOC methods fall into three main streams. (1) Image–text interaction–based methods leverage vision–language models (VLMs) to align text and image embeddings for density regression. While scalable to unseen classes, they often fail to capture fine-grained visual details, especially for atypical objects [13]. (2) Class-relevant exemplar selection discover visual patches that align with the target class by comparing arbitrarily sampled regions with class prototypes [37], but random patch sampling often produces partial or noisy exemplars. (3) To overcome

this, detection-driven exemplar selection employs open-vocabulary detectors (OVD) to propose text-conditioned boxes as candidate exemplars. However, OVDs often fail to provide clean single-instance exemplars, especially in dense scenes. For example, VA-Count [41] employs GroundingDINO [21] to extract candidate exemplars and then uses a binary filter to verify single-object instances. However, this pipeline struggles when GroundingDINO provides few or no single-instance boxes. As shown in Fig. 2(a), for the class 'apple', only a handful of valid single-instance boxes are detected, leading to an extremely limited exemplar pool. Conversely, for the category 'legos', it predicts only one large box encompassing all instances. This dependence on the detector's initial proposals creates a single point of failure that propagates through the counting pipeline. Furthermore, Fig. 2(b) illustrates that counting accuracy is highly sensitive to exemplar choice, rendering exemplar selection as a critical bottleneck. These limitations underscore the need for a principled exemplar selection strategy for ZOC.

To address this need, we introduce *CountZES*, a training-free framework for object counting via zero-shot exemplar selection, Fig. 2(c). CountZES formulates exemplar discovery as a progressive, multi-stage process comprising Detection-Anchored Exemplar (DAE), Density-Guided Exemplar (DGE), and Feature-Consensus Exemplar (FCE) stages. Each stage contributes an exemplar, resulting in a complementary set that balances textual alignment, count-driven consistency, and feature-level representativeness, respectively. The first stage, DAE, begins with a text-conditioned CLIP similarity map [29] and GroundingDINO detections. To overcome the detector's limited ability to provide clean single-instance boxes, it employs the proposed *Similarity-guided SAM-based Exemplar Selection (SSES)*, which refines coarse multi-instance detections using CLIP-guided point prompts and entropy-based optimization, isolating localized, text-aligned single-object regions. The second stage, DGE, shifts from text grounding to a density-driven self-supervised paradigm. It generates a DAE-conditioned density map and leverages *Peak-to-Point (P2P) prompting* for candidate region discovery, followed by RoI-based single-instance filtering to retain boxes whose integrated density corresponds to a single object. The most reliable exemplar is then selected through the *Pseudo-GT Guided Exemplar Selection (GGES)* module, which balances count consistency, relative to statistically inferred pseudo-ground truth (GT) count, with semantic compactness. Finally, FCE emphasizes feature-level coherence. Using the DGE exemplar as a reference, the *Feature-based Representative Exemplar Selection (FRES)* module projects each candidate onto SAM's feature space and identifies most representative exemplar via clustering.

Importantly, CountZES is a training-free framework that operates without any task-specific fine-tuning. While

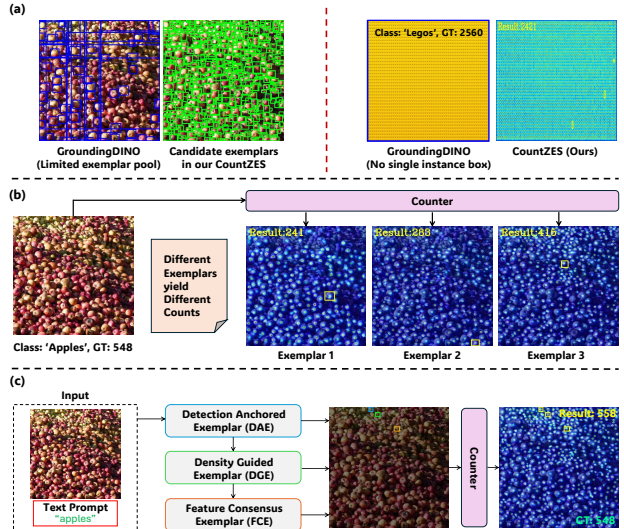


Figure 2. (a) Detectors like GroundingDINO [21] often yield very few or even fail to provide single instance boxes. (b) Counting is sensitive to exemplar choice. (c) Introducing CountZES, a training-free, multi-stage exemplar selection approach for ZOC.

it leverages pretrained VLM, segmentation, and counting models, its exemplar selection pipeline remains independent of any dataset-specific optimization. This design enables improved generalization across datasets which is validated through extensive evaluations across diverse benchmarks spanning natural, aerial and medical domains, Fig. 1. In summary, we make following contributions:

- We propose CountZES, a training-free framework for object counting via zero-shot exemplar selection across three synergistic stages (DAE, DGE, and FCE) that collectively balance textual grounding, count consistency, and feature representativeness, yielding a diverse set.
- CountZES introduces dedicated modules at each stage, with *SSES* refining multi-instance detections into precise single-instance boxes. *P2P prompting* and *RoI count-based filtering* for density-driven exemplar discovery, and *GGES* and *FRES* for exemplar refinement through pseudo GT guidance and feature-level consensus, respectively.
- Being training-free, CountZES demonstrates better generalization across datasets and even across domains. Extensive experiments across natural, aerial, and medical cell-counting benchmarks demonstrate its robustness and superior performance compared to SOTA methods.

2. Related Work

To eliminate the dependence on manually annotated exemplars in FSOC methods [3, 7, 20, 22, 30], Xu *et al.* [37] introduce the ZOC task, which estimates object counts from a class name by employing a text-conditioned variational autoencoder (VAE) that synthesizes visual exem-

plars through patch–prototype pseudo-labels. However, the arbitrary selection of patches hinders precise object delineation, thereby degrading exemplar quality. Subsequent works [1, 13, 14] leverage image–text alignment to model object–class correlations without relying on visual exemplars, enhancing scalability but often failing to preserve structural detail for irregularly shaped objects. Detection-driven approaches such as DAVE [27] adopt a detect-and-verify pipeline but bias toward majority-class counts. Recent VLM-based frameworks like PseCo [11] employs a three-stage point, segment and count design integrating SAM for segmentation and CLIP for verification, while GeCo [26] unifies detection, segmentation, and counting with a single-stage dense query encoder–decoder architecture. VA-Count [41] instead leverages GroundingDINO for text-guided detection and performs a simple logits-based exemplar selection (top-3), yielding limited exemplar diversity and relying on DINO’s initial proposals (often multi-instance boxes). Our CountZES explicitly handles the challenge of limited or no single instance boxes coming from the detector and progressive multi-stage exemplar selection offers a natural diversity in the exemplar set. Finally, T2ICount [28] exploits text-to-image diffusion priors for open-world counting but may exhibit dataset bias due to training. In contrast, our CountZES being training-free demonstrates superior generalization ability.

3. Method

We introduce CountZES, a training-free framework for ZOC (Fig. 3), which progressively discovers high-quality exemplars through three synergistic stages, namely DAE (Sec. 3.1), DGE (Sec. 3.2), and FCE (Sec. 3.3). Each stage contributes a distinct, yet complementary, perspective to exemplar selection as discussed in subsequent sections.

3.1. Detection Anchored Exemplar (DAE)

Given an image $I \in \mathbb{R}^{H \times W \times 3}$ and a text prompt t (Fig. 3), we compute CLIP similarity $S \in [0, 1]^{H \times W}$ to highlight regions semantically aligned with t , while GroundingDINO simultaneously generates text-aligned object proposals.

Initial Box Selection: Each detection box \mathbf{b}_i serves as a candidate region, within which S provides fine-grained confidence cues about semantic alignment with t . However, not all detections correspond to clean, single-instance regions, as some may encompass multiple instances or include background areas. To quantify the internal consistency of each region, we require a measure that captures how concentrated or dispersed the similarity responses are within the box. We therefore compute the *entropy* of the CLIP similarity distribution inside \mathbf{b}_i , which reflects the spatial uniformity of similarity values. Intuitively, boxes that include multiple objects or background exhibit high entropy, as similarity fluctuates across different semantic regions and ob-

ject boundaries. In contrast, a box that tightly encloses a single, well-aligned instance yields low entropy, indicating compact and coherent similarity responses in S .

Let c_i denote the confidence of the i^{th} detection from GroundingDINO, and $\widehat{H}(\mathbf{b}_i)$ the normalized entropy of similarity values within its bounding box \mathbf{b}_i . Each box is assigned a composite score balancing detection confidence and the inverse entropy term:

$$J_{\text{box}}(\mathbf{b}_i) = \alpha c_i + (1 - \alpha)(1 - \widehat{H}(\mathbf{b}_i)), \quad (1)$$

where $\alpha = 0.5$ controls the trade-off between *semantic confidence* and *spatial purity*, the latter reflecting how consistent S is within \mathbf{b}_i . Higher $J_{\text{box}}(\mathbf{b}_i)$ indicates boxes that are both confident (high c_i) and internally consistent (low \widehat{H}), favoring single-instance regions over cluttered ones. The top-scoring box, $\mathbf{b}^c = \arg \max_{\mathbf{b}_i} J_{\text{box}}(\mathbf{b}_i)$, is selected as the *coarse region of interest*. Why coarse? Although this entropy-weighted scoring favors regions with fewer overlapping instances or backgrounds, it does not guaranty that the selected box strictly contains a single instance. When all GroundingDINO detections correspond to grouped regions, even the top-scoring box may include multiple instances. Hence, this coarse selection is refined next by the similarity-guided SAM-based exemplar selection (SSES) module to obtain an instance-specific region.

Sim-guided SAM-based Exemplar Selection (SSES): Given the coarse region \mathbf{b}^c , SSES refines it into a clean, instance-specific exemplar by leveraging the similarity map S and SAM’s segmentation capability. The core intuition is that regions containing well-aligned object instances will exhibit distinct peaks in S , representing local maxima of semantic alignment with the target text. To identify high-similarity regions, we sample k peaks from S within \mathbf{b}^c by applying percentile-based threshold rather than a fixed similarity cutoff. Percentiles are computed over the full similarity map S , normalizing thresholds to each image’s global similarity statistics. Starting from a high percentile (e.g., 90th), the threshold is gradually relaxed in fixed steps ($\Delta p = 10$) until at most $k = 16$ peaks (see supplementary) are detected within \mathbf{b}^c . This adaptive relaxation dynamically adjusts the confidence level for peak selection based on the strength and density of responses in the coarse region. Formally, for a percentile p , the threshold is defined as $\tau(p) = \text{Perc}_p(S)$, and we retain spatial locations inside $\Omega(\mathbf{b}^c) = \{(x, y) \mid x_0 \leq x \leq x_1, y_0 \leq y \leq y_1\}$ whose similarity values exceed this threshold:

$$\mathcal{Q}(p) = \{q = (x, y) \in \Omega(\mathbf{b}^c) \mid S(q) \geq \tau(p)\}, \quad (2)$$

where q denotes a local peak in S , and $\mathcal{Q}(p)$ represents the set of spatial locations within \mathbf{b}^c whose similarity values surpass the global percentile threshold $\tau(p)$. This percentile-based strategy identifies strong responses across

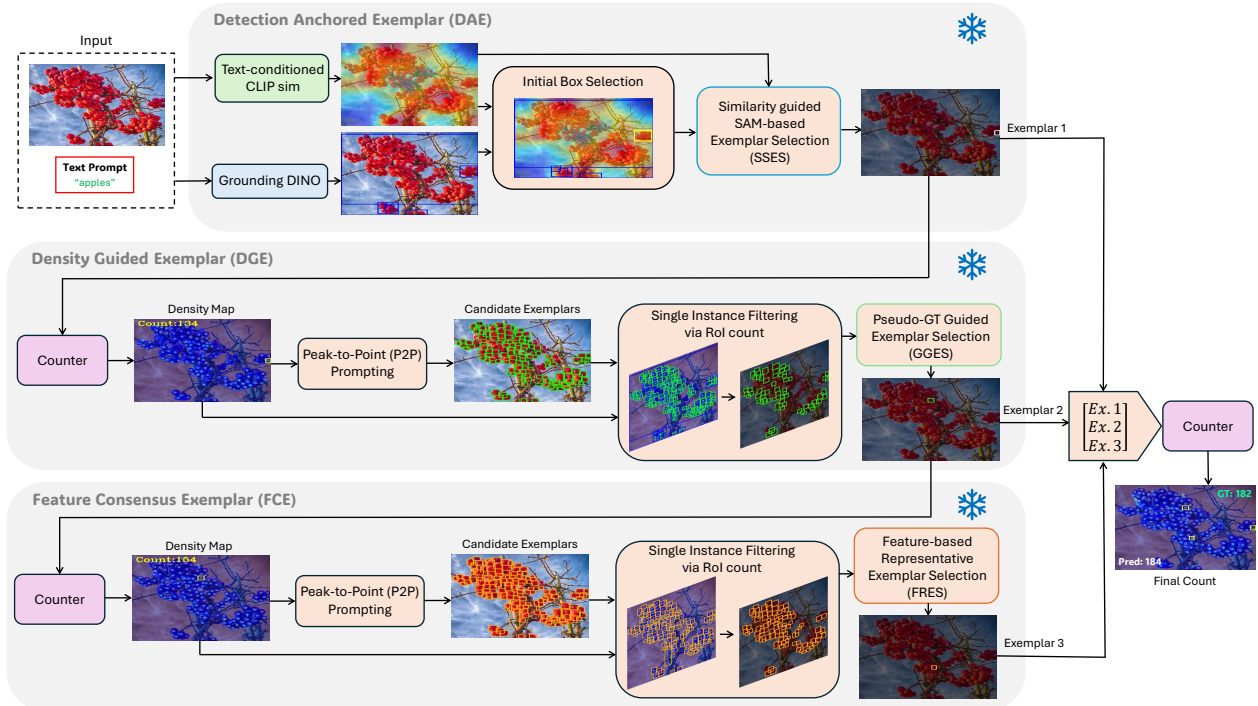


Figure 3. Overview of CountZES. The pipeline operates in three stages. DAE refines GroundingDINO detections using CLIP similarity via SSES to obtain text-aligned single-instance regions. DGE then adopts a density-driven paradigm: it generates a density map conditioned on DAE exemplar, uses P2P prompting to identify candidate exemplars, applies RoI-based single-instance filtering, and selects the most reliable exemplar through GGES. Finally, FCE focuses on visual coherence by projecting candidate exemplars onto SAM’s feature map and using FRES to select the representative exemplar. An exemplar from each stage form a diverse exemplar set for final object count.

regions, while the relaxation mechanism enables the selection of high-confidence peaks even under low-contrast similarity distributions. Each selected peak q_i is then passed as a positive point prompt to SAM, generating a binary mask $M_i = \mathcal{P}(I; q_i)$. For each mask, we compute two complementary measures: (1) *semantic strength* $\text{Sim}(M_i)$, which quantifies how strongly the pixels within M_i align with the text prompt t via the mean percentile rank of their similarity values in S , i.e., $\text{Sim}(M_i) = \frac{1}{|M_i|} \sum_{u \in M_i} r(u)$, where $r(u)$ is the percentile rank of $S(u)$; and (2) *normalized entropy* $\hat{H}(M_i)$, which captures how uniformly these similarity values are distributed. While $\text{Sim}(M_i)$ favors semantically aligned regions, $\hat{H}(M_i)$ penalizes masks with diffuse or multi-object content. Each mask is then assigned a composite score that balances the two measures:

$$J_{\text{mask}}(M_i) = w_{\text{sim}} \text{Sim}(M_i) + w_{\text{ent}} (1 - \hat{H}(M_i)), \quad (3)$$

where $w_{\text{sim}} = w_{\text{ent}} = 0.5$. The optimal mask is selected as $M_{\text{DAE}} = \arg \max_{M_i} J_{\text{mask}}(M_i)$, and its corresponding bounding box (\mathbf{b}_{DAE}) defines the refined, instance-specific region. In essence, SSES acts as a fine-grained refinement stage, transforming the coarse detector-derived region \mathbf{b}^c into a single-instance exemplar \mathbf{b}_{DAE} . When the coarse region already corresponds to a confident single instance

detection, the sampled point prompts within it consistently produce the same mask, leading SSES to retain the original region. In such cases, SSES effectively verifies rather than alters the Grounding DINO detection, confirming it as a reliable exemplar. The resulting DAE thus provides a semantically grounded and spatially refined support region used in subsequent stages of exemplar selection and counting.

3.2. Density-Guided Exemplar (DGE)

Peak-to-Point (P2P) prompting: Given the input image I and exemplar \mathbf{b}_{DAE} , the pretrained counter produces a density map $D \in \mathbb{R}^{H \times W}$, where each pixel value estimates the expected object count (Fig. 3). The total count is $C = \sum_{x,y} D(x,y)$, and local maxima in D correspond to potential object centers. Assuming D follows an approximately Gaussian distribution, most pixel responses correspond to background while object peaks appear as statistical outliers. Thus, an adaptive threshold is defined as $T_D = \mu_D + 2\sigma_D$, where μ_D and σ_D are the mean and standard deviation of D . Pixels satisfying $D(x,y) \geq T_D$ are retained as high-confidence candidates. Distinct peaks are then identified via local peak detection, which retains only the strongest responses within a fixed neighborhood,

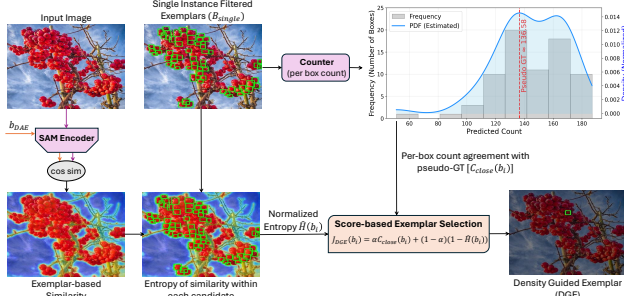


Figure 4. Overview of GGES module in the DGE stage. Per-box counts from single-instance candidates are used to estimate a pseudo-GT count via non-parametric density estimation. A SAM-based similarity map, conditioned on the DAE exemplar, captures semantic correspondence, and a composite score combining count proximity to the pseudo-GT and similarity-map entropy identifies the final density-guided exemplar.

yielding a set of spatially separated candidate points:

$$\mathcal{P} = \{ p_i = (x_i, y_i) \mid D(p_i) \geq T_D \}. \quad (4)$$

To ensure semantic consistency with GroundingDINO detections, we apply box gating, retaining only peaks p_i that fall within at least one detection box $\mathbf{b}_j^{\text{DINO}}$. The filtered prompt set is thus $\mathcal{P}^* = \{ p_i \in \mathcal{P} \mid p_i \in \Omega_{\text{DINO}} \}$, where Ω_{DINO} denotes the union of all detection boxes. Each surviving point $p_i \in \mathcal{P}^*$ is used as a positive prompt for SAM, generating a binary mask $M_i = \mathcal{P}(I; p_i)$ and its corresponding bounding box \mathbf{b}_i . These boxes then serve as candidate exemplars for subsequent selection.

Single-instance filtering via RoI count: To verify whether \mathbf{b}_i captures a single instance, we compute its integrated density within the region of interest (RoI):

$$\hat{c}(\mathbf{b}_i) = \sum_{(x,y) \in \Omega(\mathbf{b}_i)} D(x, y), \quad (5)$$

where $\Omega(\mathbf{b}_i)$ denotes the set of pixel coordinates inside the box. This operation is conceptually inspired by the *RoI pooling* mechanism in Fast R-CNN [6]. Since regression noise and density diffusion may yield fractional counts above one, boxes with predicted counts satisfying $1 < \hat{c}(\mathbf{b}_i) < 2$ are retained as single-instance candidates. The resulting subset $\mathcal{B}_{\text{single}}$ represents single-instance proposals for subsequent exemplar refinement.

Pseudo-GT guided exemplar selection (GGES): To identify the most reliable exemplar within $\mathcal{B}_{\text{single}}$, we estimate a pseudo-GT count that reflects the consensus among all single-instance candidates. Rather than relying on discrete per-box predictions $\hat{c}_i = \hat{c}(\mathbf{b}_i)$, we model their empirical distribution using a non-parametric probability density function (PDF). This continuous PDF reveals the dominant count region, consolidating multiple uncertain predictions

into a stable pseudo-GT reference (Fig. 4). By leveraging the overall distribution instead of individual estimates, this approach mitigates outlier effects and guides exemplar selection toward the statistically most consistent estimate.

Each candidate box \mathbf{b}_i is then evaluated for its closeness to the pseudo-GT count, defined as $C_{\text{close}}(\mathbf{b}_i)$. Higher $C_{\text{close}}(\mathbf{b}_i)$ indicate higher representativeness as a density-guided single-instance exemplar. However, count consistency alone does not ensure semantic purity. A region may agree with pseudo-GT yet still include clutter or background. To assess the semantic compactness of each candidate region, we compute an exemplar-conditioned SAM similarity map. Unlike the DAE stage, where a text-conditioned CLIP similarity map was used due to the absence of a concrete exemplar, the DGE stage benefits from having the previously obtained \mathbf{b}_{DAE} exemplar. This enables a more discriminative and instance-specific similarity computation. Specifically, \mathbf{b}_{DAE} is passed through SAM’s encoder to obtain its feature embedding, which is then compared, via cosine similarity, with the spatial embeddings of the entire image. The resulting similarity map provides a more discriminative and instance-specific representation, highlighting regions that share strong visual and structural correspondence with the exemplar (Fig. 4).

The normalized entropy of this similarity map within each box \mathbf{b}_i , denoted as $\hat{H}(\mathbf{b}_i)$, quantifies how spatially concentrated the exemplar’s feature activation is. Low entropy indicates compact, object-specific responses, while high entropy suggests background interference or multiple objects. Thus, $\hat{H}(\mathbf{b}_i)$ complements $C_{\text{close}}(\mathbf{b}_i)$ by ensuring the exemplar is both statistically consistent and semantically pure. Each candidate is scored as follows:

$$J_{\text{DGE}}(\mathbf{b}_i) = \alpha C_{\text{close}}(\mathbf{b}_i) + (1 - \alpha) (1 - \hat{H}(\mathbf{b}_i)), \quad (6)$$

where $\alpha = 0.5$ balances count consistency and semantic compactness. The box with the highest score is selected as DGE, $\mathbf{b}_{\text{DGE}} = \arg \max_{\mathbf{b}_i \in \mathcal{B}_{\text{single}}} J_{\text{DGE}}(\mathbf{b}_i)$. DGE thus complements the text-conditioned DAE by introducing a count-driven self-supervised perspective. By grounding exemplar selection in the predicted density rather than textual cues, DGE enhances coverage and robustness, particularly in cluttered or repetitive scenes where text-conditioned grounding alone is insufficient.

3.3. Feature-Consensus Exemplar (FCE)

While DGE enforces statistical consistency via pseudo-GT estimation, it does not explicitly capture visual coherence among candidate instances. The FCE stage refines exemplar selection at the feature level, ensuring that the final exemplar is visually representative of the dominant object appearance within the scene. Unlike DAE, which begins from text-conditioned grounding, FCE builds upon the exemplar from the DGE stage, \mathbf{b}_{DGE} . Using \mathbf{b}_{DGE} as the an-

chor, FCE regenerates a density map, and performs P2P prompting followed by single-instance filtering, mirroring the steps of DGE up to the formation of $\mathcal{B}_{\text{single}}$. However, instead of pseudo-GT guided selection, FCE introduces a *Feature-based Representative Exemplar Selection (FRES)*.

Feature-based Rep Exemplar Selection (FRES): Given the set of single-instance boxes $\mathcal{B}_{\text{single}}$, our goal is to identify the exemplar that most effectively captures the dominant visual appearance of the object class (Fig. 5). The image I is first passed through SAM’s encoder to obtain a dense feature map $\Phi \in \mathbb{R}^{256 \times 64 \times 64}$. Since projecting small boxes onto this low-resolution map may cause spatial detail loss, Φ is upsampled to $\Phi^{\text{up}} \in \mathbb{R}^{256 \times 256 \times 256}$ using window attention-based upsampling as in [36]. Each candidate box \mathbf{b}_i is then projected onto Φ^{up} , and the corresponding region $\Phi^{\text{up}}(\Omega_f(\mathbf{b}_i))$ defines its local feature subset. Finally, each box descriptor \mathbf{v}_i is computed via spatial average pooling:

$$\mathbf{v}_i = \frac{1}{|\Omega_f(\mathbf{b}_i)|} \sum_{(u,v) \in \Omega_f(\mathbf{b}_i)} \Phi^{\text{up}}(:, v, u), \quad (7)$$

The vector \mathbf{v}_i thus represents the semantic appearance of region \mathbf{b}_i in the SAM feature space. Since the magnitude of pooled features may vary with object size, texture, or illumination, direct comparison between descriptors can be biased toward high-energy regions. To mitigate this effect, we apply ℓ_2 normalization so that all descriptors lie on a unit hypersphere, ensuring that their pairwise dot products correspond to cosine similarity.

While each descriptor \mathbf{v}_i captures the visual characteristics of a single-instance region, these descriptors may still vary due to pose, scale, illumination, or minor background interference. To isolate the most representative exemplar, we cluster the descriptors in SAM’s feature space to identify the dominant appearance pattern. Specifically, we cluster \mathbf{v}_i into two groups using cosine similarity, forming a majority and a minority cluster. This partition effectively separates the visually consistent, frequently occurring appearances from peripheral or noisy ones. The majority cluster \mathcal{C}_{maj} captures the dominant object appearance, and the exemplar whose descriptor is closest to its centroid is selected as the representative exemplar, $\mathbf{b}_{\text{FCE}} = \arg \max_{\mathbf{b}_i \in \mathcal{C}_{\text{maj}}} s(\mathbf{v}_i, \mu_{\text{maj}})$. Where $s(\cdot, \cdot)$ denotes cosine similarity and μ_{maj} is the normalized mean feature of the majority cluster. The selected exemplar \mathbf{b}_{FCE} thus reflects the shared visual characteristics across all single-instance proposals. By grounding exemplar selection in feature-level consensus rather than count statistics, FCE complements DGE by emphasizing visual coherence.

Ultimately, the best exemplars obtained from DAE, DGE, and FCE collectively form the final exemplar set for counting. Selecting one exemplar per stage, rather than multiple exemplars from a single stage, introduces cross-perspective diversity (see ablations in Sec. 4). This diversity

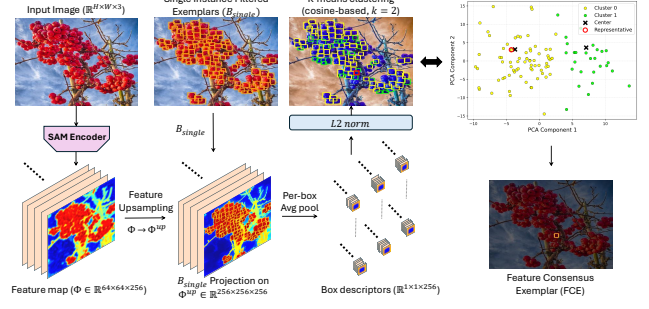


Figure 5. Overview of FRES module in the FCE stage. Single-instance boxes $\mathcal{B}_{\text{single}}$ are projected onto SAM’s upsampled feature map Φ^{up} to obtain ℓ_2 -normalized regional embeddings. These embeddings are clustered, and the box closest to the majority-cluster centroid is selected as the representative exemplar.

improves counting performance by enabling the counter to perceive object variations more comprehensively and reducing bias toward any single representation modality.

4. Experiments

Datasets and Evaluation Metrics. We evaluate our CountZES framework on diverse benchmarks including FSC-147 [31], CARPK [9], PerSense-D [33], and two medical cell-counting datasets namely, VGG [17] and MBM [25]. FSC-147 dataset contains 6,135 paired images across 147 object classes. CARPK dataset provides a bird’s-eye view of 89,777 cars across 1,448 parking-lot images, serving as a standard benchmark for assessing cross-domain generalization. The recently introduced PerSense-D dataset serves as a dense counting benchmark, comprising 717 images spanning 28 object categories, with an average of 53 target instances per image. The VGG dataset comprises 200 fluorescence microscopy images with simulated bacterial cells captured at varying focal depths. The MBM dataset includes 44 microscopic images containing 126 ± 33 nuclei per image, posing a challenging counting scenario due to high appearance variability. Following prior class-agnostic object counting works [28, 37, 41], we employ mean absolute error (MAE) to measure counting accuracy and root mean square error (RMSE) to assess model robustness.

Implementation Details. CountZES employs CLIP [29] for text–image alignment and GroundingDINO [21] for initial box proposals, with the detection threshold set to 0.15. SAM [16] is used for mask generation leveraging point prompts across the SSES, GGES, and FRES modules. To demonstrate the model-agnostic nature of CountZES, we separately utilize CounTR [20] and DSALVANet [7] as pretrained off-the-shelf few-shot object counters. When the counter is pretrained on the same dataset as the one being evaluated, we denote this configuration as *in-domain*. Under the training-free setting, CountZES employs counter pretrained on a dataset different from the one being tested.

Table 1. Comparison of CountZES with SOTA ZOC methods on FSC-147 dataset. Best results are in bold and second-best are underlined. † indicates ZOC methods based on exemplar discovery.

Method	Venue	Training	MAE	RMSE
ZSOC [†] [37]	CVPR’23	Yes	22.09	115.17
CLIP-Count [13]	ACM’23	Yes	17.78	106.62
CounTX [1]	BMVC’23	Yes	15.88	106.29
VLCounter [14]	AAAI’24	Yes	17.05	106.16
PseCo [11]	CVPR’24	Yes	16.58	129.77
DAVE [27]	ICCV’24	Yes	14.90	103.42
VA-Count [†] [41]	ECCV’24	Yes	17.88	129.31
GeCo [26]	NeurIPS’24	Yes	13.30	108.72
T2ICount [28]	CVPR’25	Yes	11.76	97.86
CountZES [†] (<i>in-domain</i>)	(Ours)	No	15.77	91.40
SAM [16]	ICCV’23	No	42.48	137.50
Count Anything [23]	arXiv’23	No	27.97	131.24
GroundingDINO [21]	ECCV’24	No	59.23	159.28
TFOC [32]	WACV’24	No	24.79	137.15
TFCAC [19]	WACV’25	No	23.59	113.60
CountZES [†]	(Ours)	No	21.09	110.14

Table 2. CountZES compared to SOTA on CARPK dataset.

Method	MAE	RMSE
CLIP-Count [13]	11.96	16.61
CounTX [1]	8.13	10.87
GroundingDINO [21]	29.72	31.60
VA-Count [41]	10.63	13.20
GeCo [26]	10.34	14.73
T2ICount [28]	8.61	13.47
CountZES (Ours)	7.24	9.22

Specifically, when evaluating on FSC-147, we use a counter pretrained on CARPK, whereas for all remaining datasets, the counter pretrained on FSC-147 is employed.

Quantitative Result on FSC-147. We evaluate CountZES under two distinct configurations as shown in Table 1. In the *in-domain* setting, DSALVNet pretrained on FSC-147 dataset is used as the counting backbone. Under this setup, CountZES achieves the best RMSE among SOTA while maintaining a competitive MAE. Compared to the leading exemplar selection-based method, VA-Count [41], CountZES lowers MAE by 11.8% and RMSE by 29.30%, indicating that the exemplars identified by our method are of higher quality. In the *training-free* setting, CountZES achieves SOTA performance with lowest MAE and RMSE.

Quantitative Result on CARPK. To evaluate cross-dataset generalization, we test CountZES on CARPK using DSALVNet as a counter pretrained on FSC-147. CountZES attains the lowest MAE and RMSE (Table 2), demonstrating remarkable transferability across domains (natural vs aerial). Notably, CountZES outperforms T2ICount [28] in generalization even though it is the current SOTA on FSC-147 dataset. This superior generalization can be attributed to our training-free design, which avoids dataset-specific bias typically introduced through training.

Table 3. CountZES compared to SOTA on PerSense-D dataset.

Method	Density-based						Class-wise	
	Low		Med		High		Overall	
	MAE	RMSE	MAE	RMSE	MAE	RMSE	MAE	RMSE
GeCo [26]	11.63	17.84	10.30	20.61	12.38	24.13	13.12	28.36
T2ICount [28]	30.04	122.91	25.16	76.95	20.62	52.23	24.95	88.21
CountZES	6.86	19.22	10.26	14.44	20.36	43.65	12.29	28.32

Table 4. Comparison of CountZES with SOTA ZOC methods on medical cell counting datasets VGG and MBM.

Method	VGG [17]		MBM [25]	
	MAE	RMSE	MAE	RMSE
GeCo [26]	67.32	77.53	92.59	104.52
T2ICount [28]	151.35	162.81	30.01	44.44
CountZES (Ours)	45.55	74.41	22.16	40.06

Table 5. Ablation study for CountZES on FSC-147 dataset: (left) stage-wise contribution; (right) demonstrates the advantage of cross-stage collaboration over single-stage exemplar selection.

DAE	DGE	FCE	MAE	RMSE	Configuration	MAE	RMSE
●	○	○	25.13	97.40	DAE only	21.73	118.03
●	●	○	20.75	92.36	DGE only	17.38	108.56
●	●	●	15.77	91.40	FCE only	19.42	116.53
					CountZES	15.77	91.40

Quantitative Result on PerSense-D. Following the same cross-dataset generalization protocol, we evaluate CountZES on the PerSense-D dataset (Table 3). In addition to overall category-wise performance, we conduct fine-grained analysis across three density-based splits; *low*, *medium*, and *high*, as defined in [33]. Compared to SOTA, CountZES demonstrates competitive performance under varying crowding conditions. Notably, 16 out of 28 classes ($\approx 57\%$) in PerSense-D overlap with FSC-147 but still T2ICount, which achieves SOTA performance on FSC-147, struggles on PerSense-D. This underscores the dataset-specific bias induced by trained models, further emphasizing our inherent generalization advantage.

Quantitative Results on VGG and MBM. To assess the cross-domain generalization capability of CountZES, we evaluate it on two medical-domain cell counting datasets: VGG and MBM. As illustrated in Table 4, CountZES achieves remarkable cross-domain performance, outperforming SOTA methods by a substantial margin.

Qualitative Result. Fig. 6 presents a qualitative comparison between CountZES and SOTA methods on diverse images, spanning natural, aerial, and medical domains. Fig. 8 further illustrates the performance of CountZES on images from FSC-147 dataset.

Ablation Study. CountZES comprises three sequential stages in its exemplar selection pipeline. Since each stage

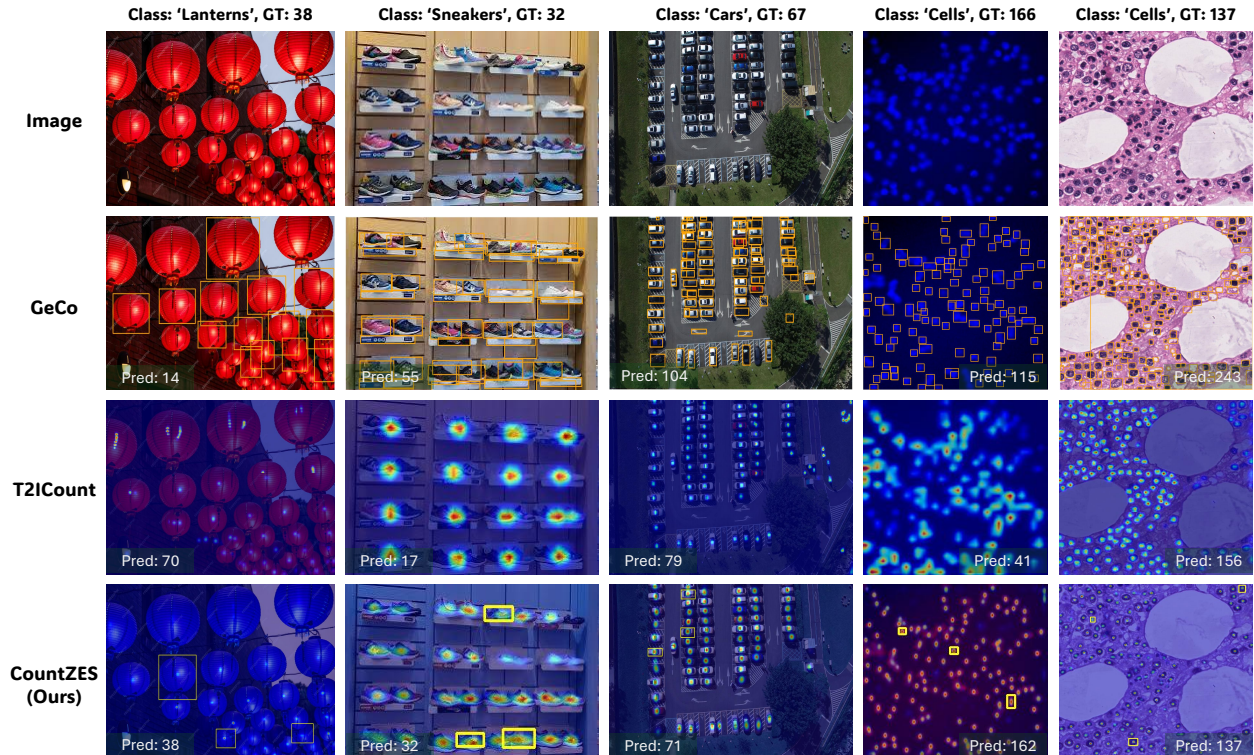


Figure 6. Qualitative comparison of CountZES with T2ICount [28] and GeCo [26] across diverse scenarios, including natural (FSC-147 [31] and PerSense-D [33]), aerial (CARPK [9]), and medical cell-counting (VGG [17] and MBM [25]) images.

builds upon the exemplar generated by the previous one, we perform a progressive ablation to quantify the incremental contribution of each stage toward overall counting performance. As shown in Table 5, adding successive stages consistently improves accuracy, validating their complementary roles. Finally, to examine the diversity induced by each stage in exemplar selection, we conduct another ablation under a consistent 3-exemplar setting by selecting the top three exemplars from each stage and comparing them against the standard CountZES configuration that uses one exemplar per stage (Table 5). The latter achieves superior performance (Fig. 7), indicating that cross-stage collaboration yields a richer, complementary, and more balanced exemplar set than any stage in isolation.

Limitation. While CountZES demonstrates better generalization across domains, certain limitations stem from the use of off-the-shelf pre-trained components like object counters and SAM. In cross-domain settings, where the pre-trained counter is trained on distributions different from the target domain, this can lead to noise in peak detection via P2P prompting. Also, as vanilla SAM lacks semantic awareness, a point prompt may yield only partial masks, capturing fragments of the object rather than complete instances. Although the scoring-based selection mechanism generally favors the most reliable exemplar at each stage, residual noise can still propagate when the majority of can-

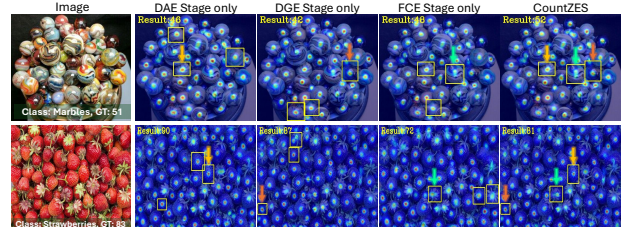


Figure 7. Demonstrates complementary nature of DAE, DGE and FCE stages. For each stage, the top three exemplars are shown with their counting outputs. One exemplar from each stage (arrows) provides complementary cues, and their combination in CountZES improves overall counting performance (last column).

didate exemplars are imperfect. As illustrated in Fig. 9 for the class “watches,” a point placed on the watch frequently segments only the dial while excluding the wristband, resulting in incomplete exemplar boxes. Additional examples in Fig. 10 highlight similar failures: for “nail polishes,” the mask captures only part of the bottle; for “comic books,” the prompt segments characters on the cover instead of the whole book; for “eggs,” SAM isolates only the yolk region; and for “sauce bottles,” it focuses on the label instead of the full object. Although the scoring mechanism generally prefers the best available candidates, residual noise can still propagate when most exemplars are imperfect. Nonethe-

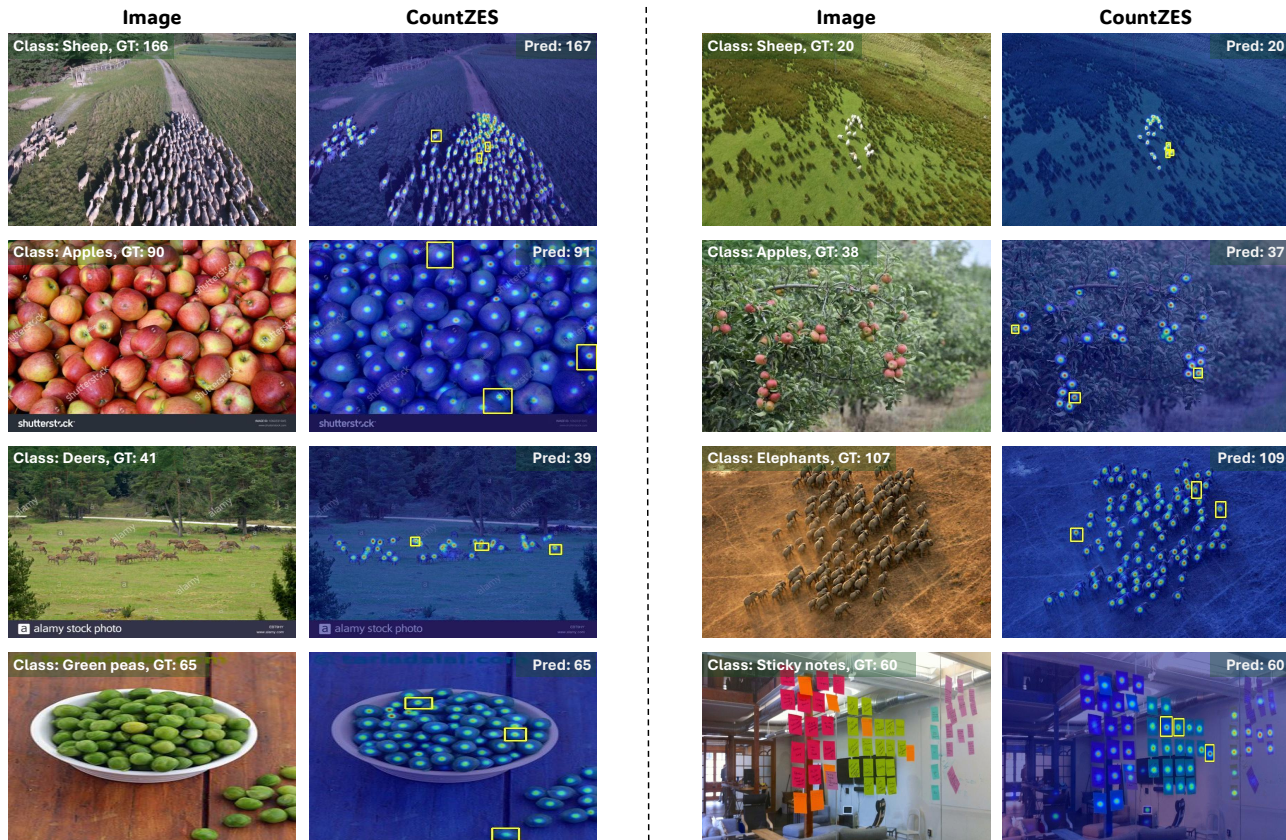


Figure 8. Qualitative results of CountZES on FSC-147 dataset.



Figure 9. Failure case illustrating CountZES selection of incomplete exemplar boxes for the class “watches.” Due to SAM’s limited semantic awareness, point prompts from density peaks segment only the watch dial, excluding the wristband, which produces partial masks and incomplete boxes that lead to suboptimal exemplar selection.

less, a key strength of CountZES lies in its modular architecture. Each component, counter or segmentation backbone, can be seamlessly replaced with more advanced alternatives without altering the overall pipeline. This flexibility opens promising avenues for further enhancing cross-domain robustness and improving exemplar fidelity in future extensions.

5. Conclusion

We presented CountZES, a training-free framework for ZOC, which formulates exemplar discovery as a three-stage

process (DAE, DGE, and FCE), each contributing complementary cues from semantic, statistical, and visual perspectives. DAE ensures text-grounded semantic alignment, DGE introduces density-driven numerical consistency, and FCE enforces feature-level consensus to identify representative exemplar. This naturally induces diversity in the exemplar set, enhancing counting performance. Extensive experiments across natural, aerial, and medical benchmarks demonstrate its superior performance compared to SOTA. CountZES challenges the conventional reliance on task-specific training and supervision, posing an open question: *Can principled exemplar selection alone be the key to scal-*



Figure 10. Additional failure cases highlighting CountZES selection of incomplete boxes as exemplars. For “nail polishes,” SAM-based point prompt segmentation in CountZES captures only partial objects; for “comic books,” point prompts isolate characters or cover details instead of the full book; for “eggs,” SAM segments only the yolk region; and for “sauce bottles,” it segments only the label instead of the whole bottle. These examples show how imperfect masks can hamper downstream exemplar selection in CountZES.

able, domain-resilient zero-shot object counting?

References

- [1] Niki Amini-Naieni, Kiana Amini-Naieni, Tengda Han, and Andrew Zisserman. Open-world text-specified object counting. In *BMVC*, 2023. 3, 7
- [2] Deepak Babu Sam, Abhinav Agarwalla, Jimmy Joseph, Vishwanath A Sindagi, R Venkatesh Babu, and Vishal M Patel. Completely self-supervised crowd counting via distribution matching. In *European Conference on Computer Vision*, pages 186–204. Springer, 2022. 1
- [3] Nikola Djukic, Alan Luke, Vitjan Zavrtanik, and Matej Kristan. A low-shot object counting network with iterative prototype adaptation. In *Proceedings of the IEEE/CVF International Conference on Computer Vision*, pages 18872–18881, 2023. 2
- [4] Adriano D’Alessandro, Ali Mahdavi-Amiri, and Ghassan Hamarneh. Afreeca: Annotation-free counting for all. In *European Conference on Computer Vision*, pages 75–91. Springer, 2024. 1
- [5] Guy Farjon, Liu Huijun, and Yael Edan. Deep-learning-based counting methods, datasets, and applications in agriculture: A review. *Precision Agriculture*, 24(5):1683–1711, 2023. 1
- [6] Ross Girshick. Fast r-cnn. In *Proceedings of the IEEE international conference on computer vision*, pages 1440–1448, 2015. 5
- [7] Jinghui He, Bo Liu, Fan Cao, Jian Xu, and Yanshan Xiao. Few-shot object counting with dynamic similarity-aware in latent space. *IEEE Transactions on Geoscience and Remote Sensing*, 62:1–14, 2024. 1, 2, 6
- [8] Michael Hobley and Victor Prisacariu. Learning to count anything: Reference-less class-agnostic counting with weak supervision. *Proceedings of the IEEE/CVF Conference on Computer Vision and Pattern Recognition*, 2023. 1
- [9] Meng-Ru Hsieh, Yen-Liang Lin, and Winston H Hsu. Drone-based object counting by spatially regularized regional proposal network. In *Proceedings of the IEEE international conference on computer vision*, pages 4145–4153, 2017. 6, 8
- [10] Yifeng Huang, Viresh Ranjan, and Minh Hoai. Interactive class-agnostic object counting. In *Proceedings of the IEEE/CVF International Conference on Computer Vision*, pages 22312–22322, 2023. 1

- [11] Zhizhong Huang, Mingliang Dai, Yi Zhang, Junping Zhang, and Hongming Shan. Point segment and count: A generalized framework for object counting. In *Proceedings of the IEEE/CVF Conference on Computer Vision and Pattern Recognition*, pages 17067–17076, 2024. 3, 7
- [12] Xiaofei Hui, Qian Wu, Hossein Rahmani, and Jun Liu. Class-agnostic object counting with text-to-image diffusion model. In *European Conference on Computer Vision*, pages 1–18. Springer, 2024. 1
- [13] Ruixiang Jiang, Lingbo Liu, and Changwen Chen. Clip-count: Towards text-guided zero-shot object counting. In *Proceedings of the 31st ACM International Conference on Multimedia*, pages 4535–4545, 2023. 1, 3, 7
- [14] Seunggu Kang, WonJun Moon, Euiyeon Kim, and Jae-Pil Heo. Vlcounter: Text-aware visual representation for zero-shot object counting. In *Proceedings of the AAAI Conference on Artificial Intelligence*, pages 2714–2722, 2024. 1, 3, 7
- [15] Muhammad Asif Khan, Hamid Menouar, and Ridha Hamila. Revisiting crowd counting: State-of-the-art, trends, and future perspectives. *Image and Vision Computing*, 129:104597, 2023. 1
- [16] Alexander Kirillov, Eric Mintun, Nikhila Ravi, Hanzi Mao, Chloe Rolland, Laura Gustafson, Tete Xiao, Spencer Whitehead, Alexander C Berg, Wan-Yen Lo, et al. Segment anything. In *Proceedings of the IEEE/CVF international conference on computer vision*, pages 4015–4026, 2023. 6, 7
- [17] Victor Lempitsky and Andrew Zisserman. Learning to count objects in images. *Advances in neural information processing systems*, 23, 2010. 6, 7, 8
- [18] Shuang Li, Faliang Chang, and Chunsheng Liu. Bi-directional dense traffic counting based on spatio-temporal counting feature and counting-lstm network. *IEEE Transactions on Intelligent Transportation Systems*, 22(12):7395–7407, 2020. 1
- [19] Yuhao Lin, Haiming Xu, Lingqiao Liu, and Javen Qinfeng Shi. A simple-but-effective baseline for training-free class-agnostic counting. In *2025 IEEE/CVF Winter Conference on Applications of Computer Vision (WACV)*, pages 8155–8164. IEEE, 2025. 7
- [20] Chang Liu, Yujie Zhong, Andrew Zisserman, and Weidi Xie. Countr: Transformer-based generalised visual counting. *arXiv preprint arXiv:2208.13721*, 2022. 1, 2, 6
- [21] Shilong Liu, Zhaoyang Zeng, Tianhe Ren, Feng Li, Hao Zhang, Jie Yang, Qing Jiang, Chunyuan Li, Jianwei Yang, Hang Su, et al. Grounding dino: Marrying dino with grounded pre-training for open-set object detection. In *European conference on computer vision*, pages 38–55. Springer, 2024. 2, 6, 7
- [22] Erika Lu, Weidi Xie, and Andrew Zisserman. Class-agnostic counting. In *Asian conference on computer vision*, pages 669–684. Springer, 2018. 2
- [23] Zhiheng Ma, Xiaopeng Hong, and Qinnan Shangguan. Can sam count anything? an empirical study on sam counting. *arXiv preprint arXiv:2304.10817*, 2023. 7
- [24] Thanh Nguyen, Chau Pham, Khoi Nguyen, and Minh Hoai. Few-shot object counting and detection. In *European Conference on Computer Vision*, pages 348–365. Springer, 2022. 1
- [25] Joseph Paul Cohen, Genevieve Boucher, Craig A Glastonbury, Henry Z Lo, and Yoshua Bengio. Count-ception: Counting by fully convolutional redundant counting. In *Proceedings of the IEEE International conference on computer vision workshops*, pages 18–26, 2017. 6, 7, 8
- [26] Jer Pelhan, Alan Lukezic, Vitjan Zavrtanik, and Matej Kristan. A novel unified architecture for low-shot counting by detection and segmentation. *Advances in Neural Information Processing Systems*, 37:66260–66282, 2024. 1, 3, 7, 8
- [27] Jer Pelhan, Vitjan Zavrtanik, Matej Kristan, et al. Dave-a detect-and-verify paradigm for low-shot counting. In *Proceedings of the IEEE/CVF Conference on Computer Vision and Pattern Recognition*, pages 23293–23302, 2024. 3, 7
- [28] Yifei Qian, Zhongliang Guo, Bowen Deng, Chun Tong Lei, Shuai Zhao, Chun Pong Lau, Xiaopeng Hong, and Michael P Pound. T2icount: Enhancing cross-modal understanding for zero-shot counting. In *Proceedings of the Computer Vision and Pattern Recognition Conference*, pages 25336–25345, 2025. 1, 3, 6, 7, 8
- [29] Alec Radford, Jong Wook Kim, Chris Hallacy, Aditya Ramesh, Gabriel Goh, Sandhini Agarwal, Girish Sastry, Amanda Askell, Pamela Mishkin, Jack Clark, et al. Learning transferable visual models from natural language supervision. In *International conference on machine learning*, pages 8748–8763. PmLR, 2021. 2, 6
- [30] Viresh Ranjan, Udbhav Sharma, Thu Nguyen, and Minh Hoai. Learning to count everything. In *Proceedings of the IEEE/CVF Conference on Computer Vision and Pattern Recognition*, pages 3394–3403, 2021. 1, 2
- [31] Min Shi, Hao Lu, Chen Feng, Chengxin Liu, and Zhiguo Cao. Represent, compare, and learn: A similarity-aware framework for class-agnostic counting. In *Proceedings of the IEEE/CVF Conference on Computer Vision and Pattern Recognition*, pages 9529–9538, 2022. 6, 8
- [32] Zenglin Shi, Ying Sun, and Mengmi Zhang. Training-free object counting with prompts. In *Proceedings of the IEEE/CVF Winter Conference on Applications of Computer Vision*, pages 323–331, 2024. 7
- [33] Muhammad Ibraheem Siddiqui, Muhammad Umer Sheikh, Hassan Abid, and Muhammad Haris Khan. Persense: Training-free personalized instance segmentation in dense images. *arXiv preprint arXiv:2405.13518*, 2024. 6, 7, 8
- [34] Harjeet Singh and Harpreet Kaur. A systematic survey on biological cell image segmentation and cell counting techniques in microscopic images using machine learning. *Wireless Personal Communications*, 137(2):813–851, 2024. 1
- [35] Aayush Kumar Tyagi, Chirag Mohapatra, Prasenjit Das, Govind Makharia, Lalita Mehra, Prathosh AP, et al. Degpr: Deep guided posterior regularization for multi-class cell detection and counting. In *Proceedings of the IEEE/CVF Conference on Computer Vision and Pattern Recognition*, pages 23913–23923, 2023. 1
- [36] Thomas Wimmer, Prune Truong, Marie-Julie Rakotosaona, Michael Oechsle, Federico Tombari, Bernt Schiele, and Jan Eric Lenssen. Anyup: Universal feature upsampling. *arXiv preprint arXiv:2510.12764*, 2025. 6
- [37] Jingyi Xu, Hieu Le, Vu Nguyen, Viresh Ranjan, and Dimitris Samaras. Zero-shot object counting. In *Proceedings of*

- the IEEE/CVF Conference on Computer Vision and Pattern Recognition*, pages 15548–15557, 2023. [1](#), [2](#), [6](#), [7](#)
- [38] Shuo-Diao Yang, Hung-Ting Su, Winston H Hsu, and Wen-Chin Chen. Class-agnostic few-shot object counting. In *Proceedings of the IEEE/CVF Winter Conference on Applications of Computer Vision*, pages 870–878, 2021. [1](#)
- [39] Wenzhe Zhai, Xianglei Xing, Mingliang Gao, and Qilei Li. Zero-shot object counting with vision-language prior guidance network. *IEEE Transactions on Circuits and Systems for Video Technology*, 2024. [1](#)
- [40] Shiwei Zhang, Qi Zhou, and Wei Ke. Enhancing zero-shot object counting via text-guided local ranking and number-evoked global attention. In *Proceedings of the IEEE/CVF International Conference on Computer Vision*, pages 21097–21106, 2025. [1](#)
- [41] Huilin Zhu, Jingling Yuan, Zhengwei Yang, Yu Guo, Zheng Wang, Xian Zhong, and Shengfeng He. Zero-shot object counting with good exemplars. In *European Conference on Computer Vision*, pages 368–385. Springer, 2024. [1](#), [2](#), [3](#), [6](#), [7](#)

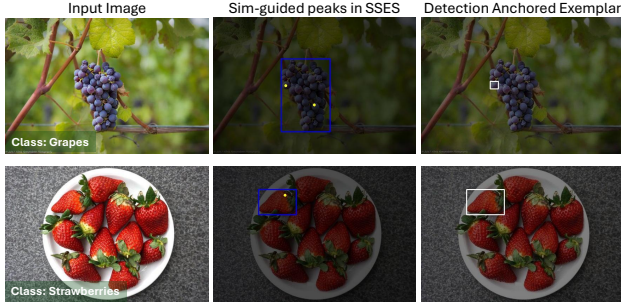


Figure 11. Visualization of SSES peak detection under multi-instance and single-instance coarse boxes. (Top row) When the initial detector box contains multiple objects, SSES identifies multiple high-similarity peaks within the coarse region, each serving as a point prompt to SAM and enabling refinement into a clean single-instance exemplar. (Bottom row) When the coarse region already corresponds to a confident single-instance detection, peak detection consistently falls on the same object, yielding a mask identical to the detector’s output. In this case, SSES functions as a verification step, retaining the original GroundingDINO box as a reliable exemplar.

A. Appendix

A.1. Ablation on k peaks in SSES module

Similarity-guided SAM-based Exemplar Selection (SSES) in Detection-Anchored Exemplar (DAE) stage, refines the initial-box selection into a clean, single-instance exemplar by jointly leveraging text-conditioned similarity map and SAM’s segmentation. It first locates the most text-aligned subregions within the coarse box by detecting high-confidence peaks in the similarity map using an adaptive percentile-relaxation strategy, ensuring robust peak detection under both strong and weak similarity patterns. As illustrated in Fig. 11 and 12, each detected peak serves as a point prompt to SAM, producing a set of candidate masks that are then evaluated using a composite score combining semantic alignment (mean percentile rank of similarities within the mask) and spatial purity (normalized entropy). This scoring mechanism prioritizes masks that are simultaneously text-consistent and instance-coherent, allowing SSES to reliably isolate single-object exemplars even in cluttered or ambiguous detections. We empirically set the maximum number of peaks at $k = 16$, which provides the best trade-off between coverage and precision for counting performance, with an ablation over $k = 4, 8, 16$ reported in Table 6.

A.2. P2P Prompting and Single-Instance Filtering

We present additional qualitative analysis illustrating the P2P prompting process and the impact of single-instance filtering. As shown in Fig. 13, given the exemplar from the DAE stage, a density map is first computed using the

Table 6. Ablation on the maximum number of similarity peaks k used in SSES during the DAE stage. $k = 16$ provides the best balance of coverage and precision, yielding the lowest MAE and RMSE for our CountZES on the FSC-147 dataset.

Method	MAE	RMSE
CountZES ($k = 4$)	16.41	91.47
CountZES ($k = 8$)	16.22	91.65
CountZES ($k = 16$)	15.77	91.40

pretrained counter conditioned on this exemplar. Peaks detected within the density map serve as point prompts to SAM, which generates corresponding masks and bounding boxes. These boxes are then filtered using RoI-count to retain only single-instance exemplars. As observed, this filtering refines the pool of candidate exemplars by discarding multi-instance or noisy regions. The resulting single-instance boxes are subsequently passed to the Pseudo-GT Guided Exemplar Selection (GGES) module to identify the final exemplar in the DGE stage.

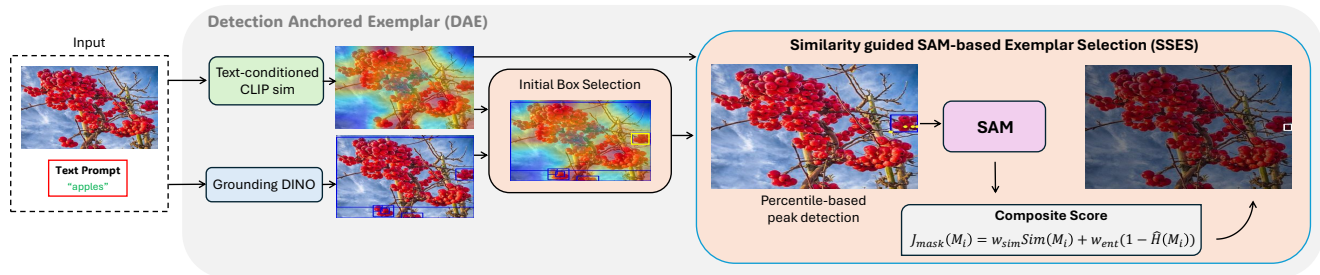


Figure 12. Illustration of the SSES module within the DAE stage. Given the detector-derived coarse box, SSES leverages the text-conditioned CLIP similarity map to identify high-confidence response peaks using an adaptive percentile-based relaxation strategy. These peaks are used as point prompts to SAM, generating multiple candidate masks. Each mask is evaluated using a composite score that balances semantic alignment and spatial purity, and the highest-scoring mask is selected as the refined single-instance exemplar. The visual pipeline highlights how similarity-driven peak sampling and mask scoring together transform a noisy coarse region into a precise exemplar.

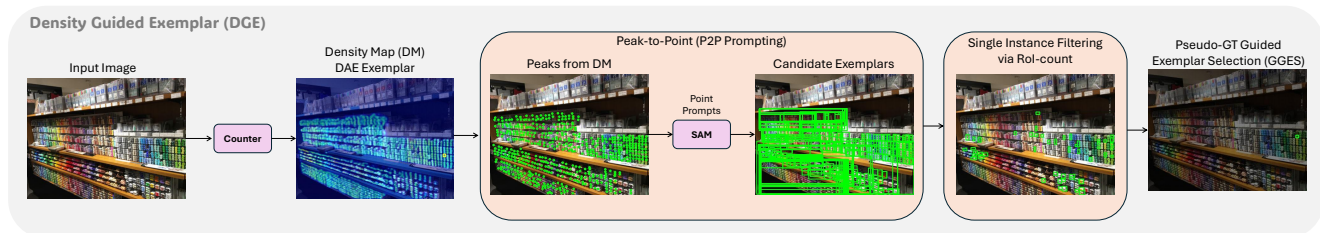


Figure 13. Overview of P2P prompting and single-instance filtering. Density peaks extracted from the density map serve as point prompts to SAM, whose masks are filtered via RoI-count to retain only single-instance regions before being passed to the GGES module for final selection in DGE stage.